Multiple Pure Tone Noise Prediction and Comparison with Static Engine Test Measurements

Fei Han*, Chingwei M. Shieh†, Anupam Sharma*, and Umesh Paliath*
G.E. Global Research Center, 1 Research Circle, Niskayuna, NY 12309, U.S.A.

This paper presents an integrated numerical procedure to predict the generation, in-duct propagation, and radiation of multiple pure tone (MPT) noise of aircraft engines. Reynolds-averaged Navier-Stokes (RANS) computational fluid dynamics (CFD) simulations using part-annulus grids have been performed to resolve the non-uniform shock signature just upstream of the fan blades. A linear superposition method is then used to reconstruct the full-annulus pressure field using the part-annulus CFD results and the as-manufactured blade stagger angles measured by a coordinate-measuring machine. In order to account for the nonlinear propagation of the shock waves inside the nacelle, a one-dimensional model has been employed to simulate the propagation of MPT from upstream of the fan leading edge to the nacelle lip. For far-field propagation, a commercially available software ACTRAN/TM is used to linearly propagate the acoustic modes to far-field microphone locations. The entire analysis process has been applied to predict MPT noise of a typical high bypass ratio engine at operating conditions when the relative tip Mach number of the fan is transonic. Comparisons against static engine test measurement are made for in-duct, near-field, and far-field sound pressure levels. Good agreement has been observed between predictions and measured data.

I. Introduction

MULTIPLE pure tone (MPT) noise, also referred to as "buzzsaw" noise, is characterized as multiple tones at frequencies that are harmonics of the engine shaft frequency. It is generated when the relative tip Mach number of the fan blade becomes transonic at the part-speed cutback condition associated with take-off and climb. At this operating condition, shocks are formed at the leading edge of the fan blade. This rotor-locked shock system rotates at the engine angular frequency and propagates nonlinearly upstream inside the engine nacelle along a helical path. In an ideal fan, all the blades will be identical, perfectly aligned, and the shock system will only contain energy in the blade passing frequency (BPF) and its harmonics. However, in reality, manufacturing processes will introduce variations in the blade geometry, resulting in shocks of non-uniform amplitudes and irregular spacing. Since the speed of a nonlinear wave is a function of its amplitude, where a stronger wave travels faster than a weaker one, minor variations in shock amplitudes and spacing are amplified with the upstream propagation distance. In frequency domain, this phenomenon can be depicted as a transfer of acoustical energy from BPF harmonics to sub-harmonics of BPFs. As a result, the sound radiated from the engine inlet exhibits multiple tones at harmonics of engine shaft rotational frequency, also known as engine-order (EO) modes.

Studies on the generation of multiple pure tones have been published by several authors since the 1970s, with the introduction of higher bypass ratio aircraft engines.[1–6] It is generally accepted that blade non-uniformities due to manufacturing variations is the dominant cause of MPT generation. Stratford and Newby[6] suggested that the variations in shock strength are attributed to blade stagger angle variations of the order 0.1^o. Similar observation has been made by Gliebe *et al.*[7] with the use of numerical analyses. On the prediction of MPT noise, Morfey and Fisher[8] calculated the non-dimensional "time of flight" of a wave spiraling around a duct in terms of the axial distance upstream of the fan, as well as the nonlinear attenuation of a regular sawtooth waveform. McAlpine and Fisher[9] proposed both time domain and frequency

*Mechanical Engineer, Energy and Propulsion Technologies, AIAA Member.
†Fluid Mechanics Engineer, Energy and Propulsion Technologies, AIAA Member.

domain numerical solution methods to study the nonlinear propagation of irregular sawtooth waveform. The frequency domain method was later extended to include liner attenuation effects[10] and validated with engine test data.[11] Another approach, based on the modified Hawking's formulation, was developed by Uellenberg[12] to account for arbitrary initial waveform spacings. In all the prediction studies mentioned above, the authors either assumed the initial irregular waveform or took the measured data as the initial solution, and only studied the nonlinear propagation of such waveform as it travels upstream inside a duct. Other researchers have studied the shock wave generation and propagation of transonic fan blades with the use of CFD.[13–15] However, they assumed identical fan blade geometries in their numerical calculations and could only analyze the nonlinear propagation and decay of shock waves at BPFs, but not MPT at sub-harmonics of BPFs.

In the current analysis, an integrated numerical procedure to predict the generation, in-duct propagation, and radiation of MPT noise is presented. Reynolds-averaged Navier-Stokes (RANS) computational fluid dynamics (CFD) simulations using measured stagger angles are performed to generate the pressure field upstream of the fan. A flow chart of the integrated prediction process is shown in Figure 1. Since the shock pattern is locked to the fan blades and rotates with the angular frequency of the shaft, steady CFD simulations in the rotating frame of reference are sufficient to resolve the flow field. A linear superposition method[7] is used to reconstruct the pressure field from arbitrary stagger angle configurations using a combination of single- and multi-passage CFD calculations. The stagger angle variations are derived from as-manufactured fan blade geometries using a coordinate-measuring machine. A more detailed explanation of this noise source prediction is provided in the next section. This pressure distribution is then used as an input to a one-dimensional non-linear propagation model developed by McAlpine and Fisher[9] to investigate the propagation of MPT to the nacelle lip. The last step in the prediction process involves the use of a commercially available acoustic software, ACTRAN/TM, to calculate the linear acoustic mode propagation from the nacelle lip to far-field locations.

The entire analysis process has been applied to predict the MPT noise of a typical high bypass ratio engine with a hardwall nacelle at operating conditions when the relative tip Mach number of the fan is transonic. Comparisons between static engine test measurements and predicted sound pressure levels at engine unsteady pressure transducer, near-field, and far-field microphone array locations are presented.

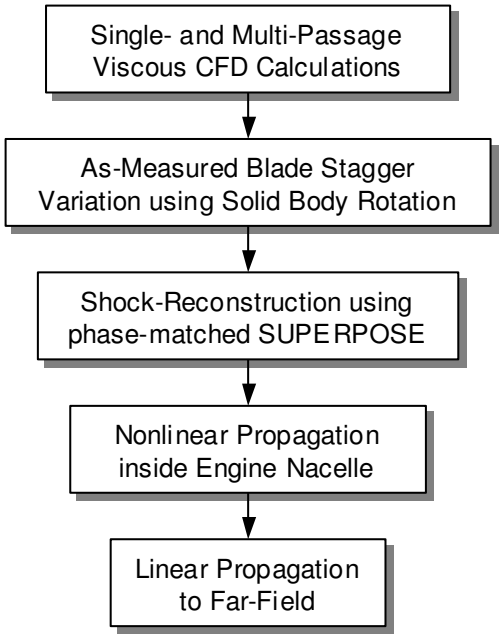

Figure 1. A flow chart of the integrated MPT prediction process.

II. Integrated MPT Prediction Methodology

In this section, the integrated MPT noise prediction process outlined in Figure 1 is described in detail. In theory, a full-annulus CFD calculation of the entire fan wheel with as-manufactured blade geometries can be performed to resolve the non-uniform shock pattern upstream of the fan. In practice, this type of calculation is still too computationally intensive for design purposes. Instead, flow solutions from a single- and a multi-passage CFD calculations are combined to create a base mode solution with one modified fan blade that models the sensitivity of the blade to manufacturing variations. It has been shown by Stratford and Newby[6] that the initial variation in shock strength is largely attributed to stagger angle variations. In order to model this variation, the modified fan blade in the multi-passage CFD calculation is rotated by 0.1^o with the use of a solid body rotation approximation, as outlined in Reference 7, to create the base mode solution. The pressure field is then reconstructed with a superposition algorithm by scaling the base mode solution with the as-manufactured stagger angle of the blades and combining the corresponding contributions in the frequency domain. In order to account for the nonlinear propagation of shock waves inside the nacelle, the modeling approach proposed by McAlpine and Fisher[9] has been employed. The far-field radiation is computed with a linear acoustic method using ACTRAN/TM.

II.A. Three-Dimensional CFD Prediction

The rotor-locked flow field is calculated with the use of an in-house 3D turbo-machinery RANS CFD solver.[16] The solver is based on a multi-block, structured, cell-centered, second-order spatial accurate finite volume scheme, with a three-stage Runge-Kutta method for time integration. A Jameson-type multi-grid scheme has been implemented to accelerate convergence. A two-equation $k-\omega$ model is employed to simulate the turbulent flow field. At both the inlet and exit boundaries of the computational domain, the Giles non-reflecting boundary conditions are applied to minimize spurious numerical reflections. Periodic boundary conditions are applied at computational domain surfaces in the circumferential direction. The number of blade passages in the multi-passage simulation has to be large enough to minimize the interaction of the modified shock with itself due to the periodic boundary condition in the circumferential direction. It has been suggested by Gliebe *et al.*[7] that a minimum of four passages are required to avoid this unphysical interaction. The exact number of passages required to fully avoid this interaction depends upon the distance upstream of the fan blade that needs to be resolved, the strength of the shock waves, and the geometry variations. In the present analysis, a six-passage CFD solution domain has been used instead.

II.B. Full-Annulus Shock Reconstruction

It has been demonstrated by Gliebe *et al.*[7] that the variations in the amplitudes of the Fourier modes composing the circumferential pressure distribution are linear with small blade geometry modifications. Previous work by Stratford and Newby[6] has shown that changes in stagger play a significant role in the generation of MPT. This observation has led to the development of a linear superposition algorithm for MPT noise source prediction with the assumptions that the MPT noise is a linear summation of the contributions from all blades and that the sound pressure levels vary linearly with the blade stagger variation. It must be emphasized that this algorithm does not model wave propagation, but only performs a reconstruction of a full-annulus pressure field using a combination of single- and multi-passage CFD calculations. With a change in stagger angle of a single blade, its two neighboring blade passages are altered. The resulting pressure variation of one blade passage can be expressed as a phase shift of the other neighboring passage due to the linearity of the system. This assumption is valid as long as the as-manufactured variation is small. This system of pressure variation from two altered blade passages due to a change in stagger angle of a single blade forms the base mode of the MPT noise. The following approach is used to derive the base mode solution.

The circumferential pressure field $p(\theta)$ at the axial location of interest may be expressed as

$$p(\theta) = p^{(1)}(\theta) + p^{(2)}(\theta), \tag{1}$$

by the assumption of linearity. Here $p^{(1)}(\theta)$ and $p^{(2)}(\theta)$ represent the effects of the adjacent modified passages. The Fourier series representation of $p(\theta)$ is

$$p(\theta) = a_0 + \sum_{i=1}^{m\times N} a_i \cos(i\theta) + b_i \sin(i\theta), \tag{2}$$

where m is an integer greater than or equal to 1, and N is the number of blades. Similarly, Fourier representations of $p^{(1)}(\theta)$ and $p^{(2)}(\theta)$ are:

$$p^{(1)}(\theta) = a_0^{(1)} + \sum_{i=1}^{m\times N} a_i^{(1)}\cos(i\theta) + b_i^{(1)}\sin(i\theta) \quad (3)$$

$$p^{(2)}(\theta) = a_0^{(2)} + \sum_{i=1}^{m\times N} a_i^{(2)}\cos(i\theta) + b_i^{(2)}\sin(i\theta). \quad (4)$$

Using the linearity assumption $p^{(2)}\theta$ can be expressed in terms of $p^{(1)}\theta$ by a phase shift of one passage ($\delta\theta$) and a negation of coefficients

$$p^{(2)}(\theta) = a_0^{(1)} + \sum_{i=1}^{m\times N}\left[-a_i^{(1)}\cos(i\delta\theta) + b_i^{(1)}\sin(i\delta\theta)\right]\cos(i\theta) + \left[-a_i^{(1)}\sin(i\delta\theta) - b_i^{(1)}\cos(i\delta\theta)\right]\sin(i\theta), \quad (5)$$

where, $\delta\theta = 2\pi/N$. The relationship between the coefficients can be written as

$$\left\{\begin{array}{c} a_i \\ b_i \end{array}\right\} = \left[\begin{array}{cc} 1-\cos(i\delta\theta) & sin(i\delta\theta) \\ -sin(i\delta\theta) & 1-\cos(i\delta\theta) \end{array}\right]\left\{\begin{array}{c} a_i^{(1)} \\ b_i^{(1)} \end{array}\right\}, \quad (6)$$

and the matrix inverted to obtain $a_i^{(1)}$ and $b_i^{(1)}$ of the base mode solution. Using these coefficients, the total pressure field due to a set of stagger variation, constituting a full-annulus fan, can be constructed by scaling the base mode solution with the specific stagger angle variation associated with each blade and summing all the blades.

In the previous analysis by Gliebe *et al.*,[7] the authors did not comment on the issue of matching the phase at the interface boundary between the one- and multi-passage CFD results. If such phase matching is not performed, as shown schematically in Figure 2(a), an artificial discontinuity in the pressure distribution will be created. This can significantly alter the base mode spectrum, resulting in an erroneous full-annulus pressure reconstruction. In order to perform phase matching, the multi-passage CFD solution is shifted to ensure C_0- and C_1-continuity at the interface. A simple linear correlation coefficient between the one- and multi-passage solutions can be calculated to determine the amount of phase shift. The result of the pressure signal reconstruction with phase matching is shown in Figure 2(b).

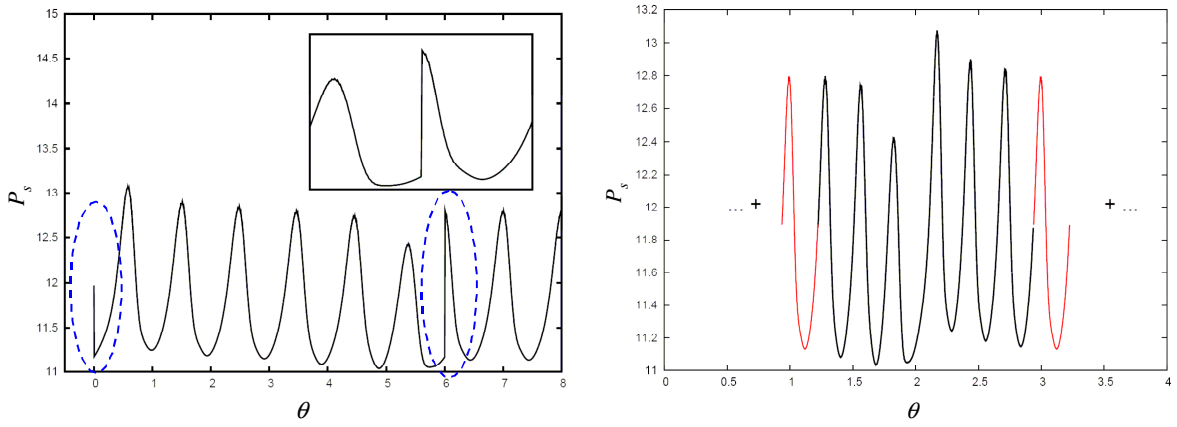

(a) Phase unmatched (b) Phase matched

Figure 2. A schematic diagram showing the relationship between the characteristic propagation direction and circumferential distance.

II.C. Nonlinear Acoustic Propagation

In order to account for the nonlinear propagation of shock waves inside the engine nacelle, the approach proposed by McAlpine and Fisher[9] is employed as part of the integrated MPT prediction methodology. It

is assumed that the direction of propagation is normal to the shock front with a constant-radial helical path along the nacelle casing, as shown in Figure 3. It has been argued by the authors that only the lowest radial order acoustic mode associated with each MPT tone is propagating inside the nacelle, while higher order acoustic radial modes are usually "cut-off".[10] This reasoning justifies the use of a one-dimensional nonlinear acoustic propagation model, and this assumption is also employed in the present analysis.

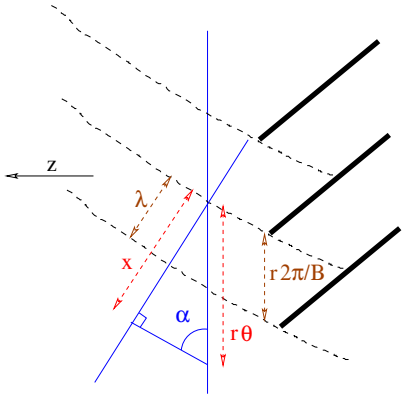

Figure 3. A schematic diagram showing the relationship between the characteristic propagation direction and circumferential distance.

In frequency domain the nonlinear propagation equation can be written as

$$\frac{\mathrm{d}C_m}{\mathrm{d}T} = \frac{im\pi}{B}\left(\sum_{l=1}^{m-1} C_{m-l}C_l + 2\sum_{l=m+1}^{\infty} C_l\tilde{C}_{l-m}\right) - \epsilon\frac{m^2}{B^2}C_m, \tag{7}$$

where m is the circumferential order of an acoustic mode, C_m is the complex amplitude of the m^{th} order mode, i.e. the amplitude of the m^{th} harmonic tone, T is a non-dimensional time, B is the number of blades, and ϵ is a dissipation factor. This equation is derived from the one-dimensional Burger's equation with the use of the following non-dimensionalizing expressions —

$$T = \frac{a_0 t}{\lambda} \qquad X = \frac{2\pi}{B}\frac{x}{\lambda} \qquad P = \frac{\gamma+1}{2\gamma}\frac{p}{P_0},$$

and converted to frequency domain in terms of a complex Fourier series,

$$P(X,T) = \sum_{m=-\infty}^{\infty} C_m(T)\ \exp\left(imX\right). \tag{8}$$

Numerical integration of Equation (7) requires truncation of the second summation term on the right-hand side of the equation. Therefore, to account for the nonlinear dissipation that occurs primarily at higher frequencies, a dissipative term is required in the equation where the amount of dissipation is determined by the term ϵ. In a subsequent paper,[10] a method to estimate the value of ϵ by analyzing the dissipation in a regular sawtooth propagation is described. The adaptive-step Runge-Kutta scheme proposed by Cash and Karp[17] is used in the current study for integrating Equation (7). The initial pressure spectrum is obtained using the linear superposition method described in previous sections.

II.D. Linear Acoustic Propagation

Once MPT noise is propagated to the nacelle lip with the use of the one-dimensional nonlinear propagation model, the far-field radiation is computed with a linear acoustic propagation method. For MPT noise, each harmonic tone of the engine shaft frequency corresponds to an acoustic mode in the nacelle. The modal circumferential order is the same as the harmonic order of the frequency. ACTRAN/TM is used to simulate the linear acoustic mode propagation from the inlet nacelle lip to far-field microphone array locations. The acoustic velocity potential is solved with a conventional finite element method (FEM) inside the computational domain and an infinite element method in the unbounded far-field domain.[18]

III. Validation and Results

Before the proposed integrated approach is applied to the prediction of MPT noise for a typical high bypass ratio aircraft engine, test cases are performed to validate the prediction algorithms and the codes developed. Full annulus two-dimensional CFD simulations at high hub-to-tip ratio with arbitrary blade stagger angles are performed, as shown in Figure 4. This eliminates the complexity of 3D flow field and as-manufactured blade geometries. In addition, the assumptions used in the 1D nonlinear acoustic propagation model also apply to the 2D CFD calculation. Comparison between superposed results and CFD simulations at typical fan operating conditions are made. If the process of phase matching described in Section II.B is not performed, it can result in artificial jumps in pressure and can significantly overpredict the sound pressure level (SPL). With proper phase matching, the comparison with full-annulus CFD is found to be in good agreement for the cases shown in Figure 5.

Validation of the nonlinear propagation model is also performed by comparing against the analytical solution of a regular sawtooth propagation obtained by Morfey and Fisher,[8] as well as full-annulus 2D CFD solutions. Figure 6 shows the comparison between the analytical solution and the nonlinear propagation model for a regular sawtooth pressure wave at various non-dimensional time, T. The numerical model is able to resolve the exponential decay of the spectral shape, as well as the decrease in amplitude as time increases. The comparison of the spectra predicted by the nonlinear model and those obtained from a direct Fourier transform of the 2D full-annulus CFD solution is shown in Figure 7. The initial waveform used in the nonlinear model is extracted from the CFD solution. This non-uniform distribution is propagated 9" upstream using the nonlinear model and then compares with the CFD solution at the same axial location. The agreement between results from the nonlinear model and the CFD solution is very favorable. Figure 8 shows comparisons of the SPL at the blade passing frequency (BPF) and its higher harmonics. The agreement between the nonlinear model and the CFD solution is in general satisfactory. While the model is able to capture the BFP harmonics of the shock as the shock propagates upstream, there are discrepancies in the amplitude. However, for EO modes, there is a good agreement between the results predicted by the model and the CFD solution. The large discrepancy at $EO = 20$ is due to insufficient grid resolution at such a high frequency, resulting in an increase in the dissipation and dispersion errors of the CFD calculation.

With a validated prediction process, the MPT noise from a typical high bypass ratio engine tested at GE Aviation's Peebles testing facility is analyzed. The predicted results are compared with the in-duct unsteady pressure transducers, near-field and far-field microphone array measurements taken during the static engine test. 3D RANS CFD calculations are performed to characterize the MPT noise source. A typical multi-block structured grid used for the flow prediction is shown in Figure 10. The grid spacing near the inlet of the computational domain is stretched to damp out spurious numerical reflections of the shock waves. A grid dependency study has been performed to determine the cell spacing requirement for accurate shock resolution upstream of the fan blade. Both one- and six-passage CFD calculations are performed at static engine operating conditions at which MPT noise was observed. Full-annulus shock reconstruction is performed as described in Section II.B using the measured stagger angle variation of the blades. The flow predictions are compared with engine test data to ensure that correct engine operating conditions are simulated, and the comparison is shown in Figure 11. The circumferential static pressure distributions at casing unsteady pressure transducer locations are extracted from the flow field solutions of the one- and six-passage CFD calculations. These distributions are used to reconstruct the full-annulus pressure field due to as-manufactured geometric variations of all the blades.

A hardwall nacelle was used in the static engine test. Two unsteady pressure transducers were installed inside the nacelle to measure dynamic pressure fluctuations on the casing. Transducer 1 and 2 are located at 1.25 and 1.74 tip chord upstream of the fan leading edge respectively. A comparison between the superposed spectrum and the measured spectrum from the first unsteady pressure transducer at 1.25 tip chord upstream of the fan leading edge is shown in Figure 12(a). It can be observed that the combination of 3D CFD and superposition prediction methodology resolves the MPT spectrum upstream of the fan with satisfactory agreement. The Fourier components of the predicted MPT spectrum are then propagated to the second transducer location using the nonlinear propagation algorithm described in Section II.C. The predicted MPT spectrum at the second transducer 1.74 tip chord upstream is then compared with the static engine test measurement, as shown in Figure 12(b). In general, there is a fair agreement between the prediction with the use of the nonlinear acoustic propagation and the test data.

Once MPT spectrum is propagated to the nacelle lip with the use of the nonlinear acoustic propagation model, the far-field radiation is computed using a linear acoustic propagation method as described in the

previous section. For MPT noise, each harmonic tone of the engine shaft frequency corresponds to an acoustic mode in the nacelle. Two microphone arrays were used in the static engine test: one is an arc of microphones at a distance of 150 feet away from the engine center; the other microphone array forms a straight line that is located much closer to the engine. The exact locations of the microphones, relative to the engine center, are shown in Figure 13. Figure 14 shows a typical computational domain used in the ACTRAN/TM simulation. Since the nacelle geometry is symmetric about the vertical engine centerline plane, only half of the nacelle geometry is modeled to reduce the computational cost. The mean flow required for the acoustic calculations is obtained using a commercial CFD software, CFX. Since the m^{th} MPT tone corresponds to the acoustic mode of circumferential order m, the predicted MPT tone amplitude from the 1D nonlinear propagation model is used directly as the amplitude of the first radial acoustic mode of the same circumferential mode order for the linear propagation process. Measured and predicted sound pressure level spectra at two microphone locations of 40^o and 80^o from the nacelle center axis at near field are plotted in Figure 15. Modes of circumferential order 1 to 5 are cut-off based on the current analysis. Therefore, only results of radiated SPLs for modes 6 to 22 are obtained. Higher order modes above engine order 22 are not simulated in the current study because a finer mesh would be required to resolve the acoustic waves accurately, and the computational time would be too expensive. It can be seen from Figure 15 that the agreement between measured data and predictions is generally favorable. The standard deviation between measurements and predictions for modes 6 to 22 are 8 and 9 dB at 40^o and 80^o respectively. Figure 16 shows the measured and predicted sound pressure level spectra at an angle of 50^o and 80^o at the 150 feet far-field microphone array. Once again only results for modes 6 to 22 are obtained by the analysis. The standard deviation between measurements and predictions for modes 6 to 22 are 8 and 7 dB at 50^o and 80^o respectively.

To further examine the accuracy of the prediction, the MPT directivity for a given EO mode at the near-field and far-field microphone array locations are plotted. Figures 17 and 18 show the measured and predicted directivity plots at the two microphone array locations for EO modes 7 and 14 respectively. At the near-field microphone location, good agreements between predictions and test data are achieved for both EO modes 7 and 14. At the far-field microphone array locations, with angles greater than 50^o, the predictions match the data very well, with standard deviation between measurements and prediction being less than 5 dB. However, the integrated numerical approach appears to under-predict the sound pressure levels compared to the test data at small angles near the nacelle center axis. One hypothesis for the under-prediction problem at small angles is the inability to account for 3D scattering in the nonlinear propagation step of the prediction process. The nonlinear propagation model has been applied for shock wave propagation from just upstream of the fan leading edge to the tip of the nacelle. For the static engine test case, the nacelle geometry is three-dimensional and includes nacelle casing with radial profile variations as well as the presence of the spinner. The mean flow field is also three-dimensional in nature. However, the assumptions of a constant one-dimensional duct and uniform mean flow have been used in 1D nonlinear model. For each frequency, only one acoustic mode with the circumferential order equal to the engine order has been assumed. In reality, due to 3D scattering effects, multiple circumferential modes would exist for a single frequency. Since EO modes of lower circumferential orders have more uniform directivities, the sound pressure level spectrum at small angles would increase if scattering effects due to 3D geometry and mean flow are included. A full 3D nonlinear acoustic propagation approach has to be employed in order to accurately model the mode scattering effects and predict the small angle radiation correctly. However, this modification has not been included in the present analysis.

IV. Summary

In this paper, an integrated numerical procedure to predict the generation, in-duct propagation, and radiation of MPT noise is developed and applied to the prediction of MPT noise from a high bypass ratio engine. The MPT base mode solution is calculated with the use of 3D RANS CFD. As-manufactured blade stagger angle variations are modeled with the use of a solid body rotation approximation. The full-annulus shock system is then reconstructed with a superposition algorithm, and propagated upstream using a 1D nonlinear acoustic propagation model inside the engine nacelle. Radiation of EO modes to far-field is performed with the use of a commercial software ACTRAN/TM. The predictions of MPT sound pressure levels are compared with measured data from unsteady pressure transducers inside the engine nacelle as well as near- and far-field microphone arrays. In general, the predictions are found to be in good agreement

with the measured static engine test data, with under-prediction of the SPL at small angles near the nacelle center axis.

Acknowledgments

The authors wish to thank colleagues from GE Aviation - Muni Majjigi, Richard Cedar, Bryan Callender, and John Wojno, and from GE Global Research - Tom Shaginaw for their encouragement and support. This project was funded under a joint GE-Boeing research effort, and we would like to thank our Boeing counterparts, namely John Premo and Cyrille Breard for making this a fruitful collaboration.

References

[1]Philpot, M. G., "The Buzz-saw Noise Generated by a High Duty Transonic Compressor," *ASME Paper No. 70-GT-54*, 1970.

[2]Hawkings, D. L., "Multiple Tone Generation by Transonic Compressors," *Journal of Sound and Vibration*, Vol. 17, No. 2, 1971, pp. 241–250.

[3]Kurosaka, M., "A Note on Multiple Tone Noise," *Journal of Sound and Vibration*, Vol. 19, No. 4, 1971, pp. 453–462.

[4]Fink, M. R., "Shock Wave Behavior in Transonic Compressor Noise Generation," *ASME Paper No. 71-GT-7*, 1971.

[5]Pickett, G. F., "Prediction of the Spectral Content of Combination Tone Noise," *Journal of Aircraft*, Vol. 9, No. 9, 1972, pp. 658–663.

[6]B. S. Stratford and D. R. Newby, "A New Look at the Generation of Buzz-saw Noise," *AIAA 77-1343*, 1977.

[7]P. Gliebe, R. Mani, H. Shin, B. Mitchell, G. Ashford, S. Salamah, and S. Connel, "Aeroacoustic Prediction Codes," *NASA/CR–2000-210244*, 2000.

[8]C. L. Morfey and M. J. Fisher, "Shockwave Radiation from a Supersonic Ducted Rotor," *The Aeronautical Journal of the Royal Aeronautical Society*, Vol. 74, 1970, pp. 579–585.

[9]A. McAlpine and M. J. Fisher, "On The Prediction of "Buzz-Saw" Noise in Aero-Engine Inlet Ducts," *Journal of Sound and Vibration*, Vol. 248, No. 1, 2001, pp. 123–149.

[10]A. McAlpine and M. J. Fisher, "On The Prediction of "Buzz-Saw" Noise in Acoustically Lined Aero-Engine Inlet Ducts," *Journal of Sound and Vibration*, Vol. 265, No. 1, 2003, pp. 175–200.

[11]A. McAlpine, M. J. Fisher, and B. J. Tester, ""Buzz-saw" noise: A Comparison of Measurement with Prediction," *Journal of Sound and Vibration*, Vol. 290, 2006, pp. 1202–1233.

[12]Uelleberg, S., "Buzzsaw noise prediction for modern turbofans," *AIAA 2004-3000*, 2004.

[13]Xu, L., "Shockwave and noise abatement of transonic fans," *ASME Paper No. GT2004-53545*, 2004.

[14]D. Prasad and J. Feng, "Propagation and decay of shock waves in turbofan engine inlets," *ASME Paper No. GT2004-53949*, 2004.

[15]Schnell, R., "Investigation of the tonal acoustic field of a transonic fanstage by time-domain CFD-calculations with arbitrary blade counts," *ASME Paper No. GT2004-54216*, 2004.

[16]D. G. Holmes, B. E. Mitchell, and C. B. Lorence, "Three-dimensional linearized Navier-Stokes calculations for flutter and forced response," *Proceedings of 8th International Symposium on Unsteady Aerodynamics and Aeroelasticity of Turbomachinery (ISUAAT), Stockholm, Sweden*, 1997.

[17]J. R. Cash and A. H. Karp, "A variable order Runge-Kutta method for initial value problems with rapidly varying right-hand sides," *ACM Transactions on Mathematical Software*, Vol. 16, No. 2, 1990, pp. 201–222.

[18]*ACTRAN User's Manual*, Free Field Technologies 2005. ACTRAN User's manual, 2005.

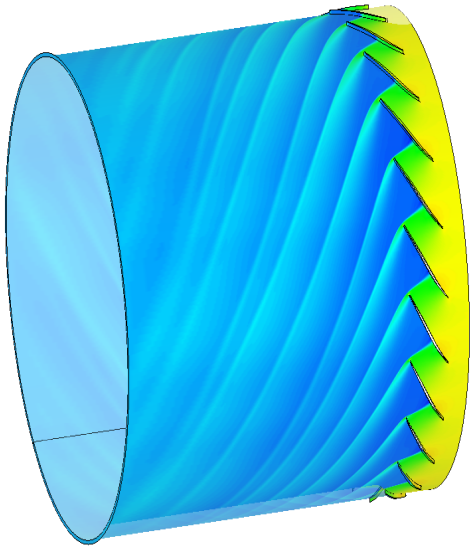

Figure 4. A 2-D full annulus simulation with stagger variation in blades to predict MPT generation.

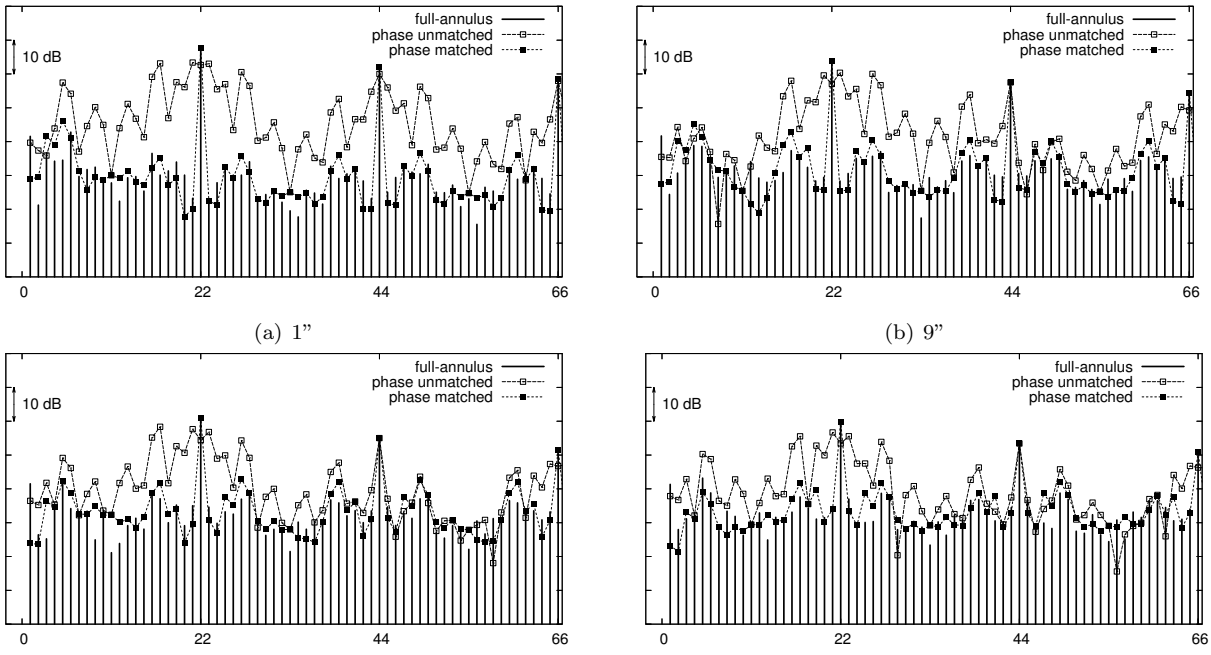

(a) 1”

(b) 9”

(c) 17”

(d) 23”

Figure 5. Validation of the linear superposition algorithm “superpose” against 2-D full-annulus simulations. Comparison presented for both phase-matched and phase un-matched results. Distance from the leading edge of the fan: (a) 1”, (b) 9”, (c) 17”, and (d) 23” .

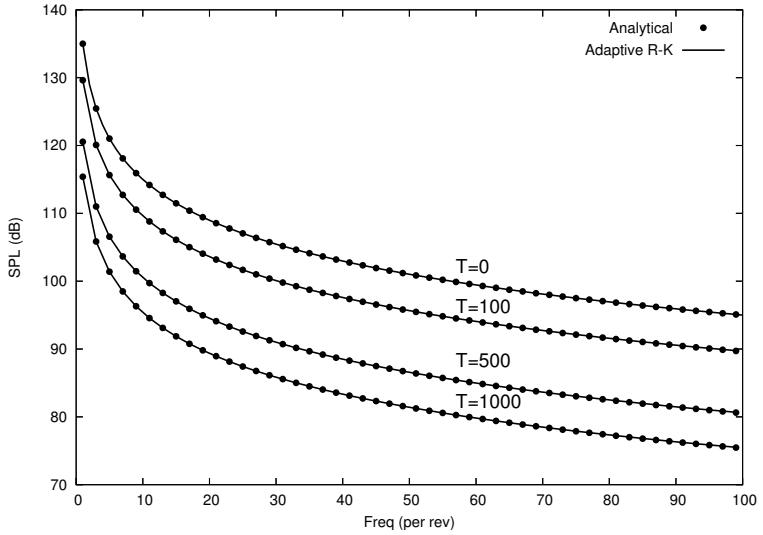

Figure 6. Validation of the nonlinear propagation model against analytical solution of a regular sawtooth propagation.

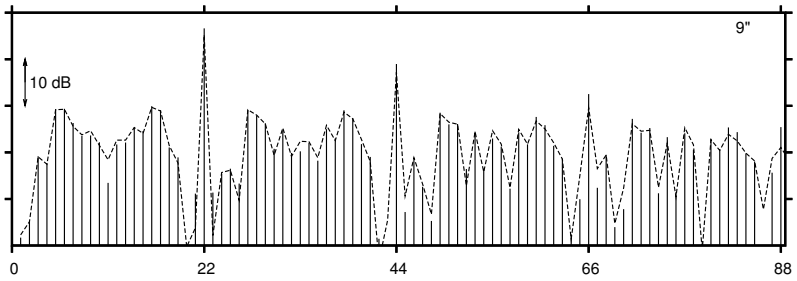

Figure 7. Comparison of spectra predicted by the nonlinear model against those obtained from direct Fourier transform of the CFD solution: — CFD, – – – nonlinear model.

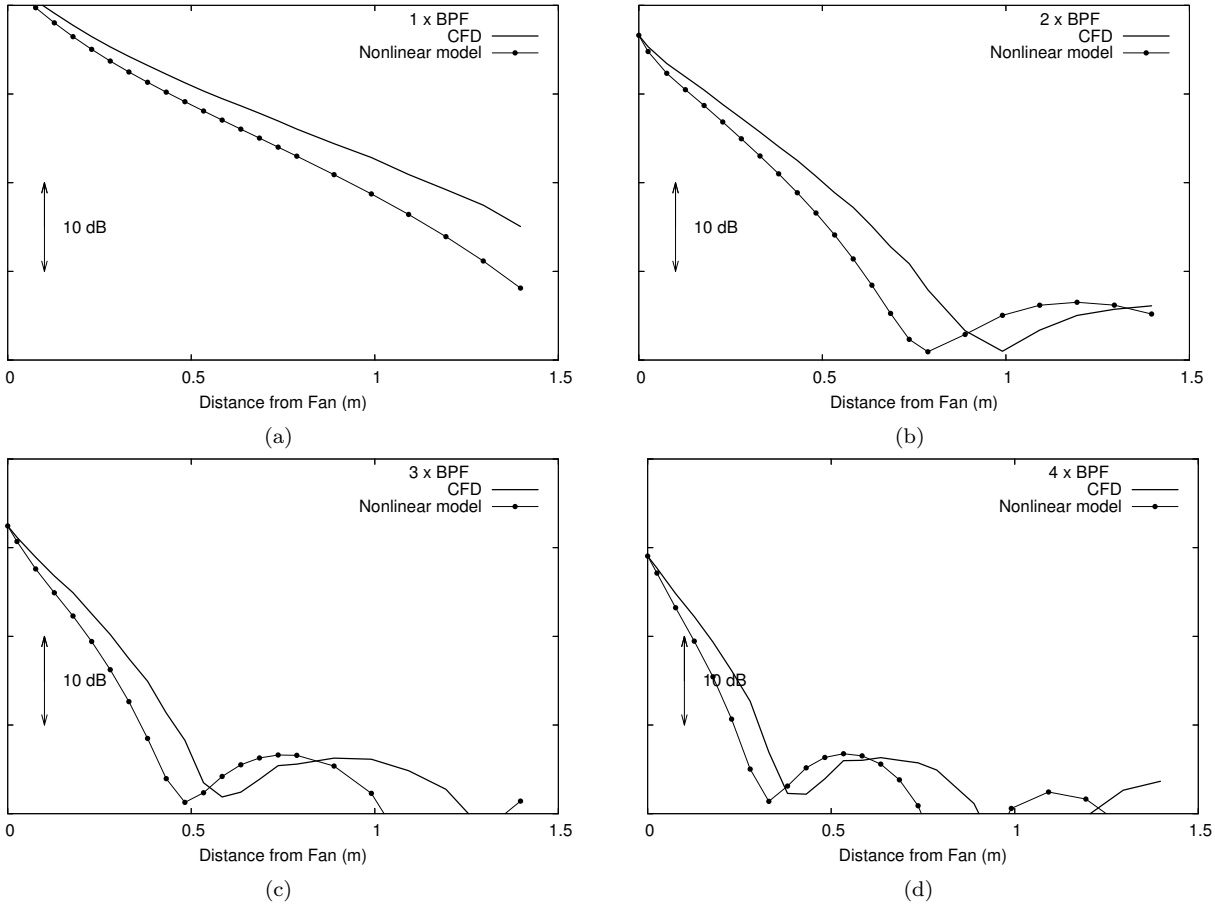

Figure 8. Comparison of harmonics of BPF predicted by the nonlinear model against those obtained from direct Fourier transform from CFD solution.

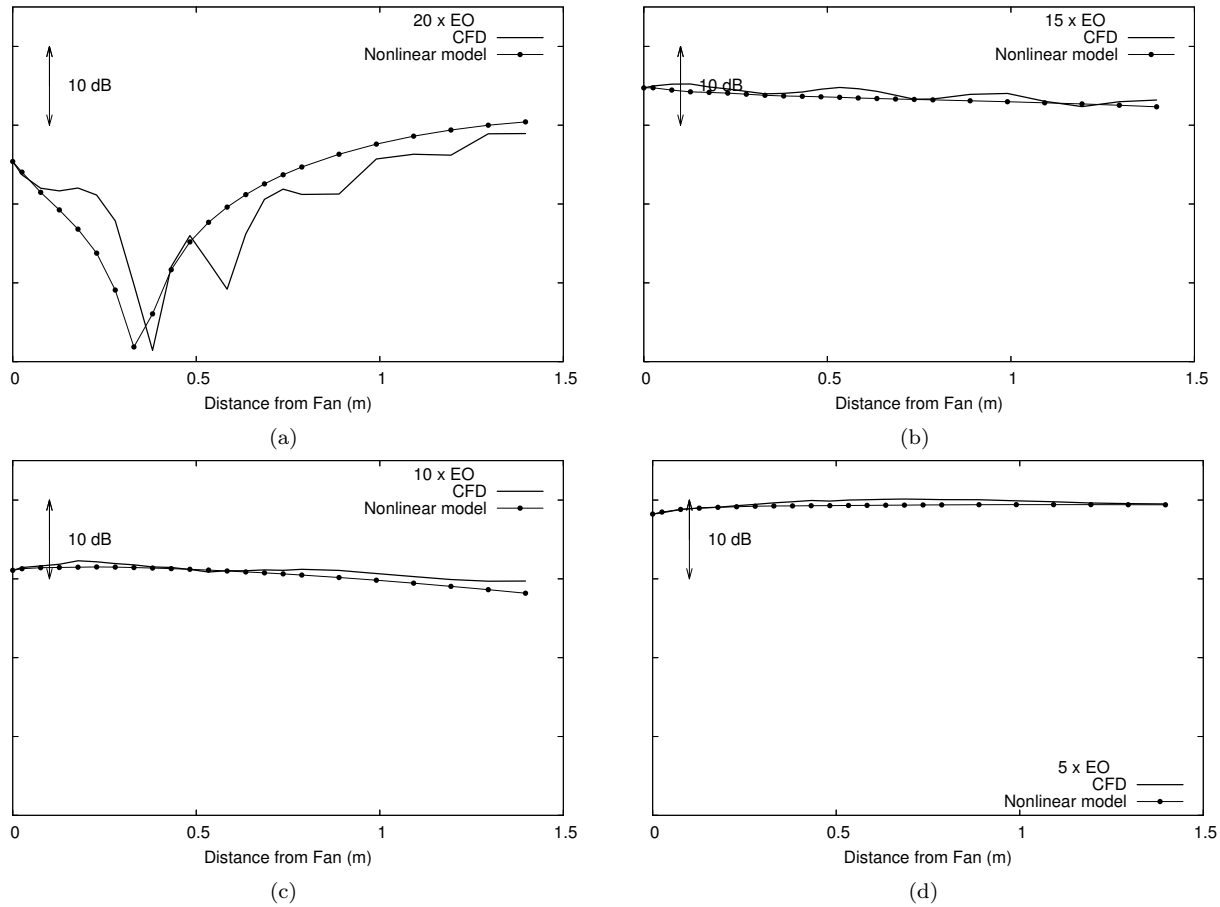

Figure 9. Comparison of EO modes predicted by the nonlinear model against those obtained from direct Fourier transform of CFD solution.

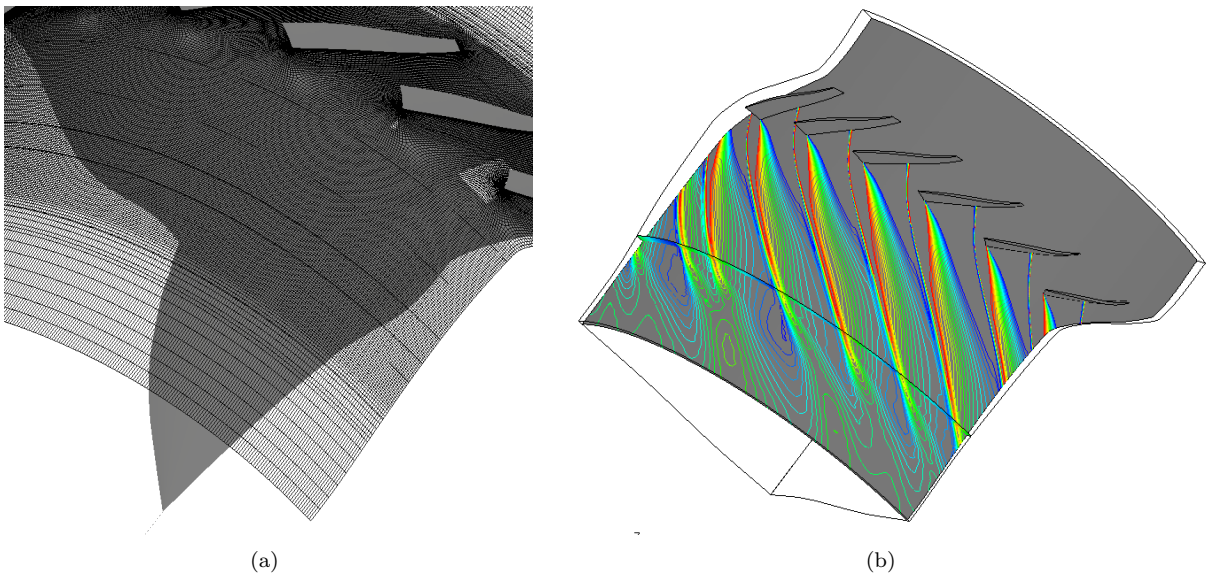

Figure 10. Computational mesh used in flow simulation: (a) Grid stretching at the inlet of the computational domain to prevent spurious numerical reflections from the inlet boundary; (b) Shock resolution upstream of the fan blade for a six-passage CFD calculation.

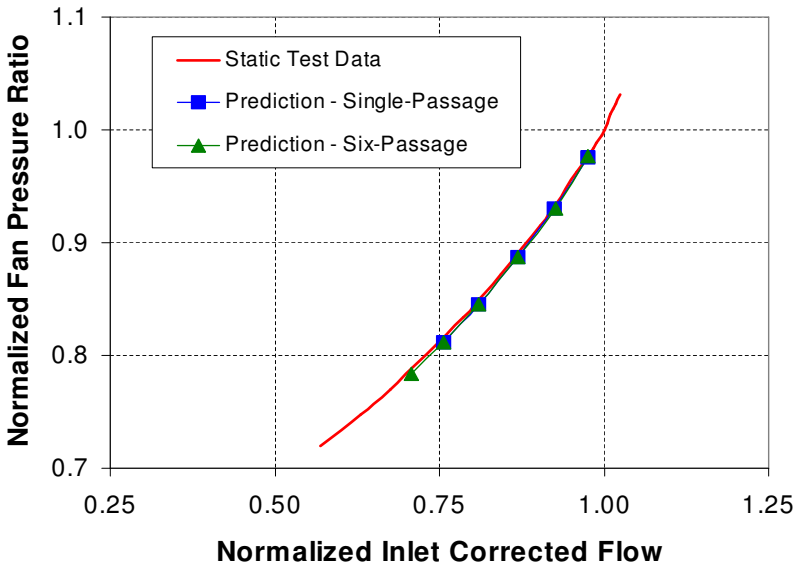

Figure 11. Comparison of 3D RANS CFD prediction of fan performance map with static engine test data

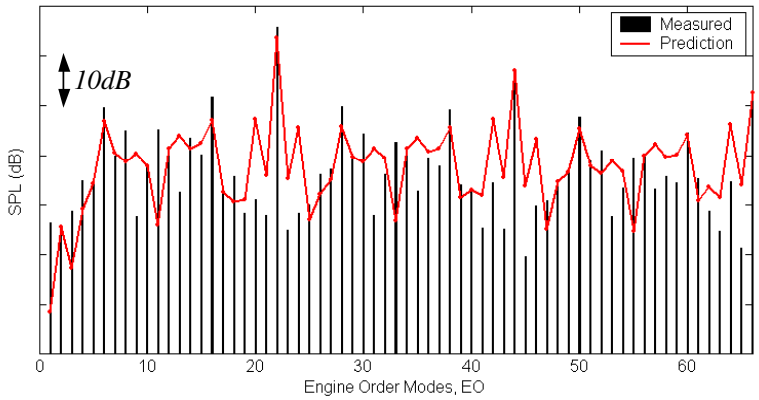

(a) 1.25 tip chord upstream of fan LE

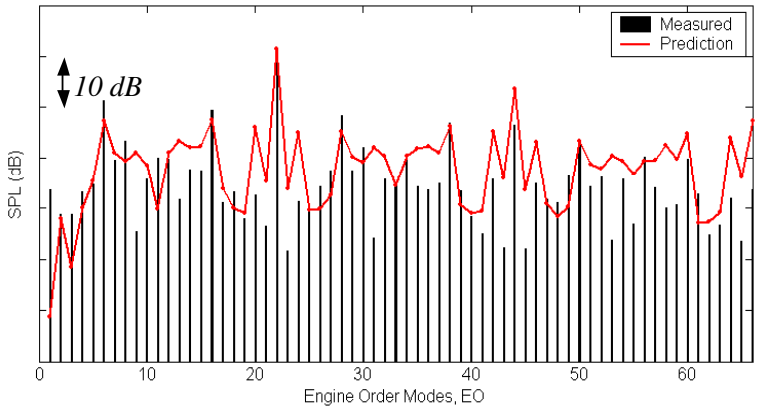

(b) 1.74 tip chord upstream of fan LE

Figure 12. Comparison of predictions using the superposition and nonlinear propagation algorithms with unsteady pressure transducer data at various axial casing locations.

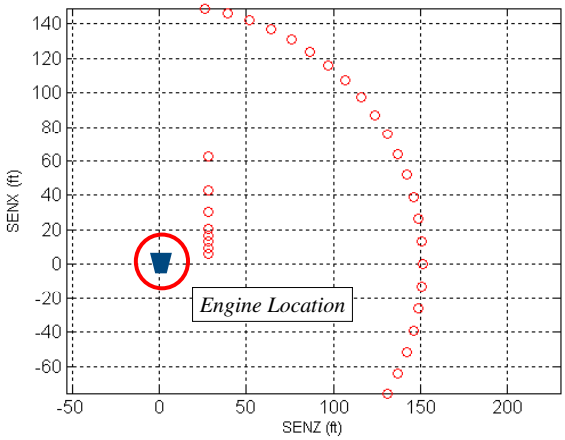

Figure 13. Microphone array locations specified in the static engine test. The engine center is at (0,0) location.

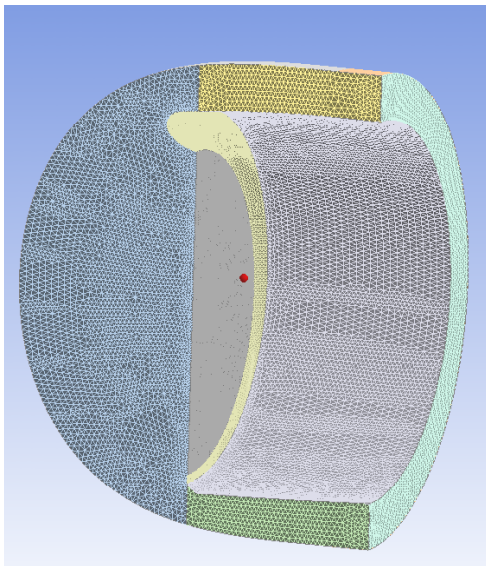

Figure 14. Computational domain used in the ACTRAN/TM simulation to propagate the MPT spectrum to far-field microphone locations.

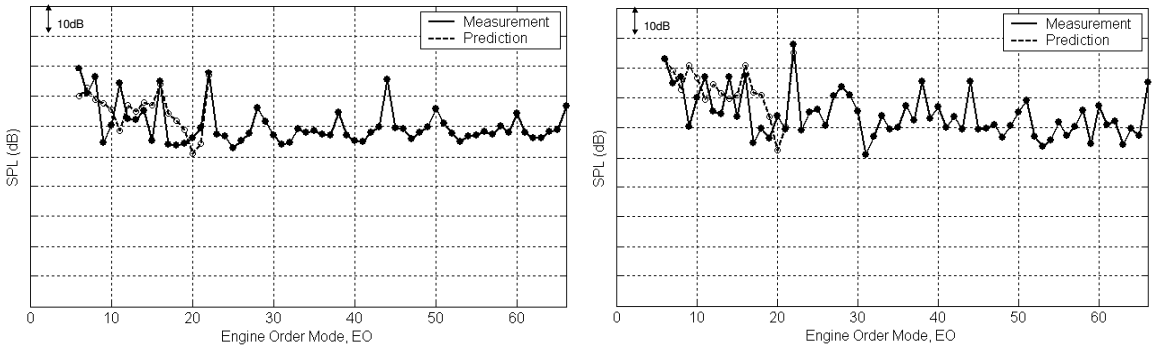

(a) 40^o (b) 80^o

Figure 15. Measured and predicted SPL spectra at (a) 40^o angle and (b) 80^o angle at near field microphone locations.

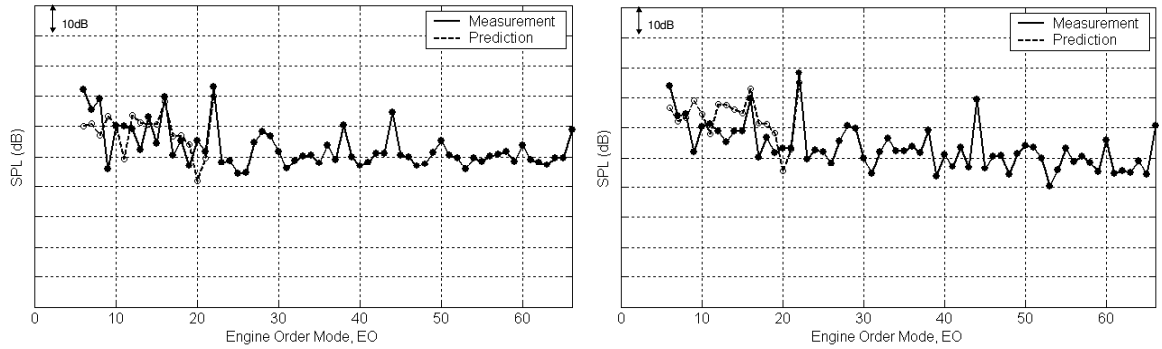

(a) 50^o (b) 80^o

Figure 16. Measured and predicted SPL spectra at (a) 50^o angle and (b) 80^o angle at far field microphone locations.

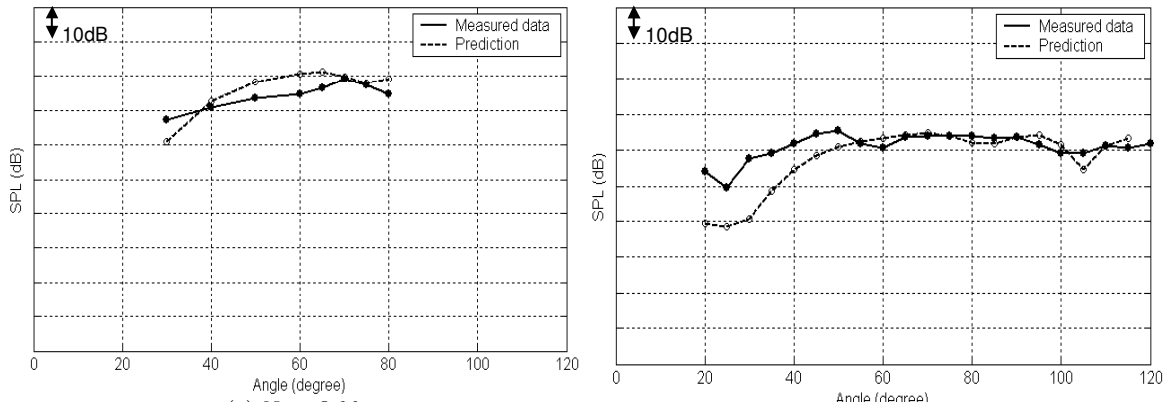

(a) Near-field (b) Far-field

Figure 17. Measured and predicted directivities for EO mode 7 near-field and far-field microphone array locations.

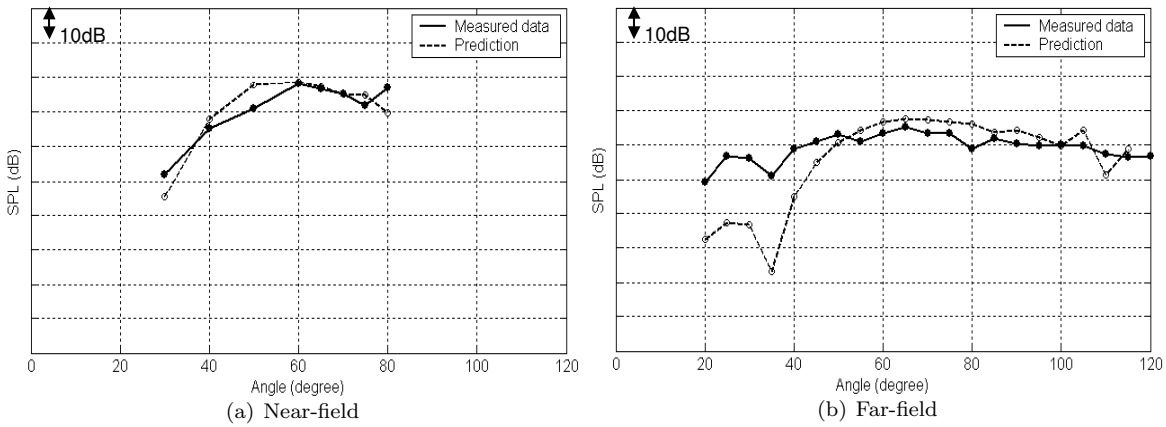

(a) Near-field (b) Far-field

Figure 18. Measured and predicted directivities for EO mode 14 near-field and far-field microphone array locations.